IEEE Access
Multidisciplinary | Rapid Review | Open Access Journal

Received April 15, 2020, accepted May 1, 2020, date of publication May 11, 2020, date of current version May 27, 2020.

*Digital Object Identifier 10.1109/ACCESS.2020.2993951*

# Antenna Modeling Using Variable-Fidelity EM Simulations and Constrained Co-Kriging

**ANNA PIETRENKO-DABROWSKA[1], (Senior Member, IEEE), AND SLAWOMIR KOZIEL[1,2], (Senior Member, IEEE)**

[1]Faculty of Electronics, Telecommunications, and Informatics, Gdansk University of Technology, 80-233 Gdansk, Poland
[2]Engineering Optimization and Modeling Center, Department of Engineering, Reykjavik University, 101 Reykjavik, Iceland

Corresponding author: Anna Pietrenko-Dabrowska (anna.dabrowska@pg.edu.pl)

This work was supported in part by the Icelandic Centre for Research (RANNIS) under Grant 206606051, and in part by the National Science Centre of Poland under Grant 2018/31/B/ST7/02369.

**ABSTRACT** Utilization of fast surrogate models has become a viable alternative to direct handling of full-wave electromagnetic (EM) simulations in EM-driven design. Their purpose is to alleviate the difficulties related to high computational cost of multiple simulations required by the common numerical procedures such as parametric optimization or uncertainty quantification. Yet, conventional data-driven (or approximation) modeling techniques are severely affected by the curse of dimensionality. This is a serious limitation when it comes to modeling of highly nonlinear antenna characteristics. In practice, general-purpose surrogates can be rendered for the structures described by a few parameters within limited ranges thereof, which is grossly insufficient from the utility point of view. This paper proposes a novel modeling approach involving variable-fidelity EM simulations incorporated into the recently reported nested kriging modeling framework. Combining the information contained in the densely sampled low- and sparsely sampled high-fidelity models is realized using co-kriging. The resulting surrogate exhibits the predictive power comparable to the model constructed using exclusively high-fidelity data while offering significantly reduced setup cost. The advantages over conventional surrogates are pronounced even further. The presented modeling procedure is demonstrated using two antenna examples and further validated through the application case studies.

**INDEX TERMS** Antenna design, surrogate modeling, kriging interpolation, co-kriging, electromagnetic (EM) simulation.

## I. INTRODUCTION

Full-wave electromagnetic (EM) simulation has become the single most important tool in a practical design of contemporary antenna structures. Apart from the rough conceptual development, EM analysis is ubiquitous throughout all other design stages, including parametric studies (conducted to verify the relevance of the introduced topological modifications and to yield a reasonable initial design for further tuning) as well as the final parameter adjustment [1], [2].

Depending on the size of the computational domain, topological complexity of the antenna (affecting, among others, the mesh grading), or the necessity of including environmental components into the analysis (connectors, housing, other radiators [3], [4]), the computational cost of EM analysis can be high. In the context of simulation-based design procedures, this may become a serious bottleneck, especially if numerous analyzes are required. Examples of the time consuming tasks include parametric optimization (both local and global [5]–[8]) but also statistical analysis [9], [10]. Expediting design procedures that require repetitive references to the EM model has been the subject of extensive research over the recent years. Available solutions include incorporation of adjoint sensitivities into gradient-based routines [11], [12], algorithmic improvements of conventional methods (e.g., suppression of finite-differentiation sensitivity updates [13], [14]), exploring response features (e.g., [15], [16]), or utilization of surrogate models, both physics-based (space mapping [17], manifold mapping [18], adaptive response scaling [19]) and data-driven (response

The associate editor coordinating the review of this manuscript and approving it for publication was Bilal Khawaja.

surfaces [20], kriging [21], neural networks [22]), as well as machine learning techniques [23], [24].

Surrogate-assisted optimization procedures normally construct the models on the fly, e.g., along the optimization path, through appropriately devised correction-prediction loops [17]. In many cases, obtaining globally accurate models is not of concern [25]. On the other hand, the idea of replacing EM analysis by the surrogate in its entirety is an appealing one because it opens the door to carry out virtually any simulation-based design task without incurring significant computational expenses. Approximation models are especially attractive in this respect due to their versatility and a wide range of specific techniques available, e.g., radial basis functions (RBF) [26], kriging [21], neural networks [22], or polynomial chaos expansion [9]. Yet, the construction of design-ready surrogates of antenna structures is beyond the capacity of conventional methods because of the dimensionality issues and a typically high-nonlinearity of antenna characteristics. Some techniques developed to alleviate these difficulties to a certain extent include high dimensional model representations (HDMR) [27], orthogonal matching pursuit (OMP) [28] or variable-fidelity modeling, e.g., co-kriging [29], two-stage Gaussian process regression GPR [30]. As a matter of fact, utilization of variable-fidelity methods has been growing, both in the context of generic surrogate modeling (e.g., [31]–[36]) but also single- [37] and multi-objective optimization [38]).

Recently, performance-driven modeling has been proposed as a way of overcoming the deficiencies of the standard techniques [39], [40]. The principal idea is to confine the surrogate domain to a region containing high-quality designs (w.r.t. the selected figures of interest), and only allocate the training data and identify the surrogate therein. This paper combines the latest of these developments, the performance-driven modeling within a constrained domain with the use of two-level kriging surrogates (i.e., the nested kriging technique of [41]), with variable-fidelity EM simulation models to further reduce the computational cost of surrogate model construction. Blending of low- and high-fidelity data is realized using co-kriging [29]. Demonstration examples indicate superiority of the proposed method over both conventional models and single-fidelity nested kriging as well as a possibility of rendering design-ready surrogates at the cost corresponding to less than two hundred high-fidelity antenna simulations.

## II. MODELING APPROACH

This section formulates the proposed modeling approach. The outline of its basic components (nested kriging [41] and co-kriging [29]) is followed by the description of the overall modeling flow.

### A. NESTED KRIGING

The nested kriging framework constructs the first-level surrogate to establish the domain for the second-level (final) model [41]. The domain is allocated to only contain designs

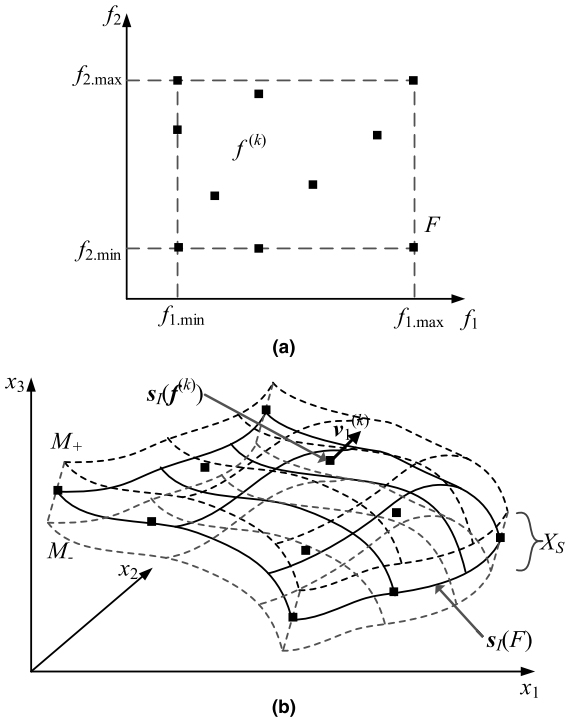


**FIGURE 1.** Conceptual illustration of the nested kriging modeling (here, shown for 2-dimensional objective space and 3-dimensional parameter space) [41]: (a) reference designs and the objective space $F$; (b) the image $s_I(F)$ of the first-level surrogate and the normal vector $v_{1(k)}$ at $f^{(k)}$; the manifolds $M_-$ and $M_+$ as well as the surrogate model domain $X_S$ defined as the orthogonal extension of $s_I(F)$.

that are of high quality w.r.t. the relevant antenna performance figures denoted as $f_k$, $k = 1, \ldots, N$. These may be related to the electrical characteristics of the antenna (e.g., operating frequency) but also material parameters (e.g., permittivity or height of the substrate the antenna is realized on). The ranges $f_{k.\min} \leq f_{k(j)} \leq f_{k.\max}$, $k = 1, \ldots, N$, to be covered by the surrogate, determine the objective space $F$.

The first-level model $\boldsymbol{s}_I(\boldsymbol{f})$ maps $F$ into the design space $X = [\boldsymbol{l}, \boldsymbol{u}]$ (an interval delimited by the lower bounds $\boldsymbol{l}$ and upper bounds $\boldsymbol{u}$ for the design variables). The training data for $\boldsymbol{s}_I$ $\{\boldsymbol{f}^{(j)}, \boldsymbol{x}^{(j)}\}_{j=1,\ldots,p}$, where $\boldsymbol{x}^{(j)} = [x_1^{(j)} \ldots x_n^{(j)}]^T$, are the reference designs optimized for the performance vectors $\boldsymbol{f}^{(j)} = [f_1^{(j)} \ldots f_N^{(j)}]$ (cf. Fig. 1), i.e., $\boldsymbol{x}^{(j)} = \text{argmin}\{\boldsymbol{x}: U(\boldsymbol{x}, \boldsymbol{f}^{(j)}\}$; here, $U$ is a scalar merit function quantifying the design utility. The set $\boldsymbol{s}_I(F) \subset X$ is an approximation of the region containing the designs optimum w.r.t. $\boldsymbol{f} \in F$. The domain is supposed to contain all such designs, therefore, an enlargement of $\boldsymbol{s}_I(F)$ is necessary [41]. It is realized by an orthogonal extension of $\boldsymbol{s}_I(F)$ towards its normal vectors, denoted at $\boldsymbol{f}$ as $\{\boldsymbol{v}_n^{(k)}(\boldsymbol{f})\}$, $k = 1, \ldots, n - N$.

The fundamental component of the surrogate domain are the manifolds $M_+$ and $M_-$ (i.e., the shifted versions of $\boldsymbol{s}_I(F)$)

$$M_{\pm} = \left\{ \boldsymbol{x} \in X : \boldsymbol{x} = \boldsymbol{s}_I(\boldsymbol{f}) \pm \sum\nolimits_{k=1}^{n-N} \alpha_k(\boldsymbol{f}) \boldsymbol{v}_n^{(k)}(\boldsymbol{f}) \right\} \quad (1)$$

with the extension factors $\alpha_k$ defined as

$$\boldsymbol{\alpha}(\boldsymbol{f}) = [\alpha_1(\boldsymbol{f}) \ \ldots \ \alpha_{n-N}(\boldsymbol{f})]^T = \\ = 0.5T\left[|\boldsymbol{x}_d \boldsymbol{v}_n^{(1)}(\boldsymbol{f})| \ \ \ldots \ \ |\boldsymbol{x}_d \boldsymbol{v}_n^{(n-N)}(\boldsymbol{f})|\right]^T \quad (2)$$

where $\boldsymbol{x}_d = \boldsymbol{x}_{\max} - \boldsymbol{x}_{\min}$ (parameter variations within $\boldsymbol{s}_I(F)$) with $\boldsymbol{x}_{\max} = \max\{\boldsymbol{x}^{(k)}, k = 1, \ldots, p\}$ and $\boldsymbol{x}_{\min} = \min\{\boldsymbol{x}^{(k)}, k = 1, \ldots, p\}$, whereas $T$ is a thickness parameter.

Using these, the domain $X_S$ is defined as

$$X_S = \left\{ \begin{array}{c} \boldsymbol{x} = \boldsymbol{s}_I(\boldsymbol{f}) + \sum_{k=1}^{n-N} \lambda_k \alpha_k(\boldsymbol{f}) \boldsymbol{v}_n^{(k)}(\boldsymbol{f}) : \boldsymbol{f} \in F, \\ -1 \le \lambda_k \le 1, \ k = 1, \ldots, n-N \end{array} \right\} \quad (3)$$

The final (second-level) kriging surrogate is rendered in $X_S$ using $\{\boldsymbol{x}_{B(k)}, \boldsymbol{R}(\boldsymbol{x}_{B(k)})\}_k = 1, \ldots, NB$, where $\boldsymbol{R}$ is the EM antenna model, and $\boldsymbol{x}_{B(k)}$ are the training samples. The sampling and model optimization procedures are described in [41].

A remark should be made with regard to the computational cost of the surrogate acquisition of the reference designs that are required for a domain confinement through the nested kriging. A designer has to decide whether this overhead is justified depending on a particular case and taking into account the actual cost of acquiring these designs. In some cases, the reference designs may be available beforehand from the prior work on the same structure. As it is shown by the results provided in Section III, building a reliable conventional surrogate may proof impossible due to dimensionality issues or wide intended parameter ranges surrogate is to be valid for. Thus, the initial cost of finding the reference designs may be unavoidable.

### B. CO-KRIGING

Incorporation of variable-fidelity EM simulation data is realized by co-kriging [29]. This section gives a brief exposition of kriging and co-kriging surrogates. We denote by $X_B = \{\boldsymbol{x}^1, \boldsymbol{x}^2, \ldots, \boldsymbol{x}^{NB}\}$ the training sample set and by $\boldsymbol{R}_f(X_B)$ the corresponding high-fidelity model outputs. The kriging surrogate $\boldsymbol{s}_{KR}(\boldsymbol{x})$ is defined as

$$\boldsymbol{s}_{KR}(\boldsymbol{x}) = \boldsymbol{M}\gamma + r(\boldsymbol{x}) \cdot \boldsymbol{\Psi}^{-1} \cdot (\boldsymbol{f}(X_B) - \boldsymbol{F}\gamma) \quad (4)$$

where $\boldsymbol{M}$ is a $N_B \times t$ model matrix of the training set $X_B$ and $\boldsymbol{F}$ is a $1 \times t$ vector of the evaluation point $\boldsymbol{x}$ ($t$ stands for the number of terms used in the regression function [29]); $\gamma$ are the regression function coefficients

$$\gamma = (X_B^T \boldsymbol{\Psi}^{-1} X_B)^{-1} X_B \boldsymbol{\Psi}^{-1} \boldsymbol{f}(X_B) \quad (5)$$

whereas $r(\boldsymbol{x}) = (\psi(\boldsymbol{x}, \boldsymbol{x}_{KR}^1), \ldots, \psi(\boldsymbol{x}, \boldsymbol{x}_{KR}^{N_{KR}}))$ is an $1 \times N_B$ vector of correlations between $\boldsymbol{x}$ and $X_B$, $\boldsymbol{\Psi} = [\Psi_{i,j}]$ is a correlation matrix with $\Psi_{i,j} = \psi(\boldsymbol{x}_{KR}^i, \boldsymbol{x}_{KR}^j)$. A popular class of correlation functions is

$$\psi(\boldsymbol{x}, \boldsymbol{x}') = \exp\left(\sum_{k=1}^{n} -\theta_k |x^k - x'^k|^P\right) \quad (6)$$

Here, $n$ is the parameter space dimensionality, whereas $P$ determines the prediction 'smoothness'; $\theta_k$, $k = 1, \ldots, n$, are hyperparameters. Typically, $P$ is constant, whereas $\theta_k$ are determined using Maximum Likelihood Estimation (MLE) [29] as

$$(\theta_1, \ldots, \theta_n) = \arg\min -(N_B/2)\ln(\hat{\sigma}^2) - 0.5\ln(|\Psi|) \quad (7)$$

where

$$\hat{\sigma}^2 = (\boldsymbol{R}_f(X_B) - F\alpha)^T \boldsymbol{\Psi}^{-1} (\boldsymbol{R}_f(X_B) - F\alpha)/N_B \quad (8)$$

and $|\Psi|$ stands for the determinant of $\boldsymbol{\Psi}$. A Gaussian correlation function ($P = 2$) is suitable for many practical problems. If no extrapolation is required, one sets $\boldsymbol{F} = [1 \ldots 1]^T$ and $\boldsymbol{M} = 1$.

Co-kriging requires rendering of the two models: $\boldsymbol{s}_{KRc}$ set up using the low-fidelity data $(X_{Bc}, \boldsymbol{R}_c(X_{Bc}))$, and $\boldsymbol{s}_{KRf}$ generated on the residuals $(X_{Bf}, \boldsymbol{r})$, where $\boldsymbol{r} = \boldsymbol{R}_f(X_{Bf}) - \rho \cdot \boldsymbol{R}_c(X_{Bf})$, here, $\rho$ is a part of the MLE of the second model. $\boldsymbol{R}_c(X_{Bf})$ can also be approximated as $\boldsymbol{R}_c(X_{Bf}) \approx \boldsymbol{s}_{KRc}(X_{Bf})$.

The configuration of $\boldsymbol{s}_{KRc}$ and $\boldsymbol{s}_{KRf}$ can be adjusted independently. Both models use (6) as a correlation function as well as a constant regression function $\boldsymbol{F} = [1\ 1 \ldots 1]^T$, $\boldsymbol{M} = 1$.

The co-kriging surrogate $\boldsymbol{s}_{CO}(\boldsymbol{x})$ is defined as

$$\boldsymbol{s}_{CO}(\boldsymbol{x}) = \boldsymbol{M}\gamma + r(\boldsymbol{x}) \cdot \boldsymbol{\Psi}^{-1} \cdot (\boldsymbol{r} - \boldsymbol{F}\gamma) \quad (9)$$

where the matrices $\boldsymbol{M}$, $\boldsymbol{F}$, $r(\boldsymbol{x})$ and $\boldsymbol{\Psi}$ can be written as

$$r(\boldsymbol{x}) = [\rho \cdot \sigma_c^2 \cdot r_c(\boldsymbol{x}), \rho^2 \cdot \sigma_c^2 \cdot r_c(\boldsymbol{x}, X_{B_f}) + \sigma_d^2 \cdot r_d(\boldsymbol{x})] \quad (10)$$

$$\boldsymbol{\Psi} = \begin{bmatrix} \sigma_c^2 \boldsymbol{\Psi}_c & \rho\, \sigma_c^2 \boldsymbol{\Psi}_c(X_{Bc}, X_{Bf}) \\ \rho\, \sigma_c^2 \boldsymbol{\Psi}_c(X_{Bf}, X_{Bc}) & \rho^2 \sigma_c^2 \boldsymbol{\Psi}_c(X_{Bf}, X_{Bf}) + \sigma_d^2 \boldsymbol{\Psi}_d \end{bmatrix} \quad (11)$$

and $\boldsymbol{M} = [\rho \boldsymbol{M}_c \ \boldsymbol{M}_d]$ where $(\boldsymbol{F}_c, \sigma_c, \boldsymbol{\Psi}_c, \boldsymbol{M}_c)$ and $(\boldsymbol{F}_d, \sigma_d, \boldsymbol{\Psi}_d, \boldsymbol{M}_d)$ are matrices obtained from $\boldsymbol{s}_{KRc}$ and $\boldsymbol{s}_{KRf}$, respectively [29].

### C. MODELING FRAMEWORK

The overall flow of the modeling process has been shown in Fig. 2. As elaborated on before, the nested kriging is primarily used to determine the surrogate domain $X_S$ (cf.Section II.A). Subsequently, co-kriging allows for combining information contained in sparsely sampled high-fidelity and densely sampled low-fidelity data (cf. Section II.B).

## III. DEMONSTRATION EXAMPLES

This section provides numerical verification of the proposed modeling approach, benchmarking against conventional surrogates and the single-fidelity nested kriging, as well as application examples (antenna optimization).

### A. CASE I: WIDEBAND MONOPOLE ANTENNA

The first example is the monopole antenna of Fig. 3(a). The structure employs a quasi-circular radiator and a modified ground plane for bandwidth enhancement [42]. The variables are $\boldsymbol{x} = [L_0 \ dR \ Rr_{rel} \ dL \ dw \ L_gL_1 \ R_1 \ dr \ c_{rel}]^T$. The EM models are implemented in CST: low-fidelity model $\boldsymbol{R}_c$

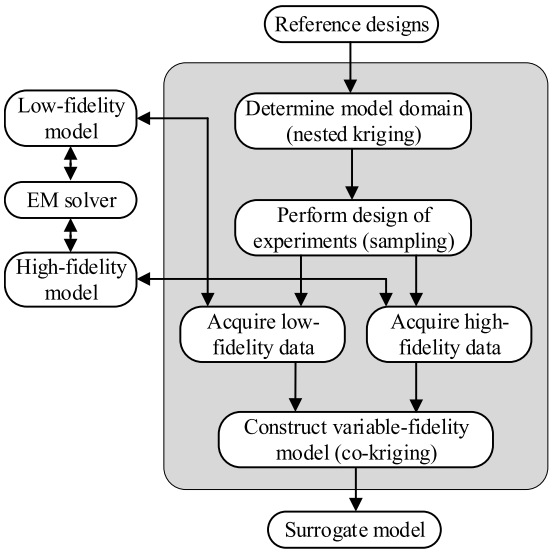


**FIGURE 2.** Variable-fidelity modeling by means of nested co-kriging: a flowchart.

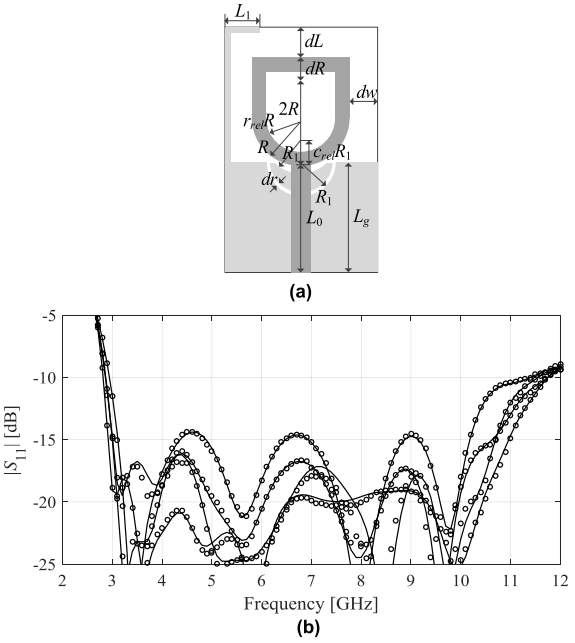


**FIGURE 3.** Wideband monopole antenna [42]: (a) geometry (ground plane shown using light gray shade), (b) reflection responses at the selected test designs: EM model (–), nested co-kriging surrogate with $N_f = 50$ and $N_c = 400$ (o).

(∼380,000 mesh cells, simulation time 56 seconds), high-fidelity model $\boldsymbol{R}_f$ (∼1,800,000 cells, 400 seconds). The models incorporate the SMA connectors. The simulations were performed on Intel Xeon 2.1 GHz dual-core CPU with 128 GB RAM.

The optimum design is the one that minimizes the reflection within the UWB frequency range from 3.1 GHz to 10.6 GHz.

The surrogate model is to be constructed within the objective space defined by the following ranges of the surrogate parameters: permittivity $2.0 \leq \varepsilon_r \leq 5.0$ and height 0.5 mm $\leq h \leq 1.5$ mm. The reference designs correspond to all combinations of $\varepsilon_r \in \{2.0, 3.5, 5.0\}$ and $h \in \{0.5, 1.0, 1.5\}$ mm. The lower and upper bounds for design variables, $\boldsymbol{l} = [11.0\ 0.0\ 5.0\ 0.10\ 3.0\ 5.5\ 11.0\ 0.6\ 2.0\ 0.2\ 0.2]^T$, and $\boldsymbol{u} = [13.5\ 0.9\ 7.\ 0.25\ 5.0\ 7.5\ 12.7\ 3.6\ 4.0\ 0.55\ 0.9]^T$, are derived from the reference points.

The nested co-kriging model has been constructed using various numbers of high- and low-fidelity samples $N_f$ and $N_c$: $N_f = 20$ and $N_c = 400$, $N_f = 50$ and $N_c = 400$, $N_f = 100$ and $N_c = 400$, as well as $N_f = 50$ and $N_c = 800$. The predictive power of the proposed variable-fidelity model is compared to that of the surrogates set up with the sole use of the high-fidelity data: conventional surrogates (kriging and RBF), as well as the nested kriging model. The kriging model has been constructed using the DACE toolbox of [44], whereas the RBF model was based on the in-house implementation (Gaussian basis functions with the scaling parameter adjusted using cross-validation).

Table 1 gathers the numerical results. Note that the constrained models (nested kriging and co-kriging) exhibit significantly better accuracy than the conventional surrogates. Furthermore, the accuracy of the proposed nested co-kriging is comparable to that of the high-fidelity nested kriging obtained using 400 and 800 samples. At the same time, the computational cost of training data acquisition is lower than for the high-fidelity nested kriging model. It is expressed in terms of the total equivalent number of $\boldsymbol{R}_f$ samples used to set up the surrogate, which are calculated as $N_f + N_c/m$, $m$ being the ratio of the simulation time between the high-fidelity model $\boldsymbol{R}_f$ and the low-fidelity model $\boldsymbol{R}_c$. In the proposed variable-fidelity framework, data acquisition cost is only between 76 and 162 equivalent high-fidelity model evaluations, depending on the setup (i.e., $N_f$ and $N_c$), see Table 1. The antenna reflection responses at the selected test designs are shown in Fig. 3(b) for the model set up using 50 high-fidelity and 400 low-fidelity samples. The plots demonstrate a very good visual agreement between the surrogate and the EM-simulated characteristics.

**TABLE 1.** Modeling results for wideband antenna.

| Number of high-fidelity samples $N_f$ | Relative RMS error | | | | | | |
|---|---|---|---|---|---|---|---|
| | Conventional models | | Nested kriging model | Variable-fidelity nested co-kriging model [this work]* | | | |
| | kriging | RBF | | $N_f = 20$, $N_c = 400$ | $N_f = 50$, $N_c = 400$ | $N_f = 100$, $N_c = 400$ | $N_f = 50$, $N_c = 800$ |
| 50 | 62.5 % | 65.1 % | 10.8 % | | | | |
| 100 | 48.5 % | 51.2 % | 7.9 % | | | | |
| 200 | 37.3 % | 38.7 % | 6.4 % | 7.6 % [**76**#] | 5.2 % [106#] | **4.3** % [156#] | 5.0 % [162#] |
| 400 | 32.4 % | 33.5 % | 5.9 % | | | | |
| 800 | 22.7 % | 24.6 % | 5.4 % | | | | |

*$N_f$ and $N_c$ stand for the number of high- and low-fidelity samples, respectively.
#The number is brackets is the total equivalent number of $\boldsymbol{R}_f$ samples used to set up the surrogate (calculated as $N_f + N_c/m$ where $m$ is the time evaluation ratio between $\boldsymbol{R}_f$ and $\boldsymbol{R}_c$).

**TABLE 2. Wideband monopole: Optimization results.**

| Target substrate | | Geometry parameter values [mm]* | | | | | | | | | | |
|---|---|---|---|---|---|---|---|---|---|---|---|---|
| $\varepsilon_r$ | $h$ [mm] | $L$ | $dR$ | $R$ | $r_{rel}$ | $dL$ | $dw$ | $L_g$ | $L_1$ | $R_1$ | $dr$ | $c_{rel}$ |
| 2.5 | 1.5 | 12.2 | 0.08 | 7.21 | 0.10 | 4.60 | 6.00 | 12.3 | 1.86 | 3.90 | 0.20 | 0.54 |
| 4.4 | 1.5 | 12.5 | 0.00 | 5.27 | 0.16 | 4.66 | 6.79 | 11.9 | 0.80 | 2.64 | 0.25 | 0.80 |
| 3.38 | 0.76 | 11.8 | 0.11 | 6.15 | 0.10 | 3.77 | 6.07 | 11.6 | 1.94 | 2.30 | 0.21 | 0.58 |
| 4.4 | 1.0 | 11.7 | 0.02 | 5.68 | 0.12 | 4.17 | 6.65 | 11.3 | 1.62 | 2.20 | 0.30 | 0.57 |

* Variables with substripct $r$ are relative, i.e., unitless.

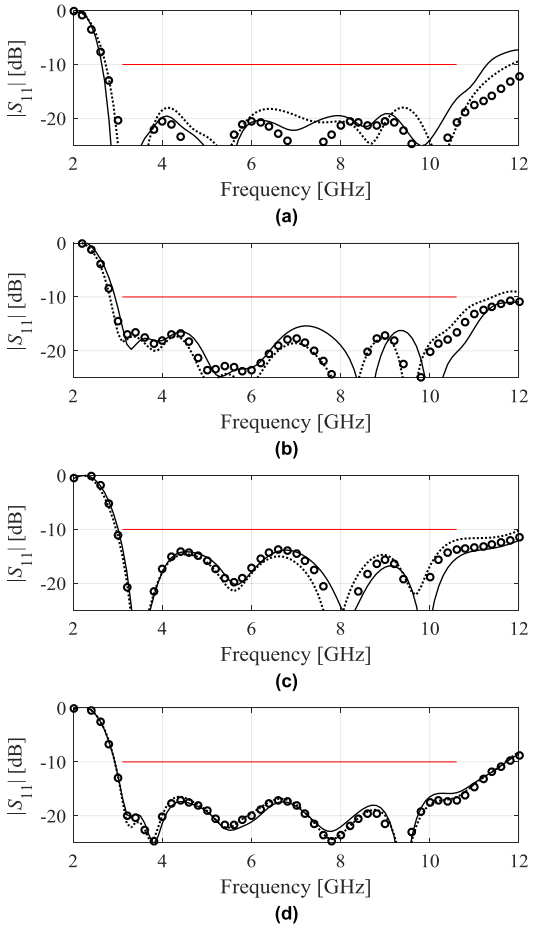


**FIGURE 4. Reflection responses of the antenna of Fig. 3 optimized using the proposed surrogate set up with $N_f = 100$ and $N_c = 400$: initial design (· · ·), surrogate response at the optimized design (o), EM simulated response (—): (a) $\varepsilon_r = 2.5$, $h = 1.5$ mm, (b) $\varepsilon_r = 4.4$, h = 1.5 mm, (c) $\varepsilon_r = 3.38$, $h = 0.76$ mm, (d) $\varepsilon_r = 4.4$, $h = 1.0$ mm. The red solid horizontal line marks the design requirements, i.e., the maximum allowed level of antenna reflection within its operating frequency range.**

For additional validation, the surrogate obtained for $N_f = 100$ and $N_c = 400$ has been optimized for various substrate parameters. Table 2 provides the numerical results, whereas Fig. 4 shows the initial and optimized antenna characteristics.

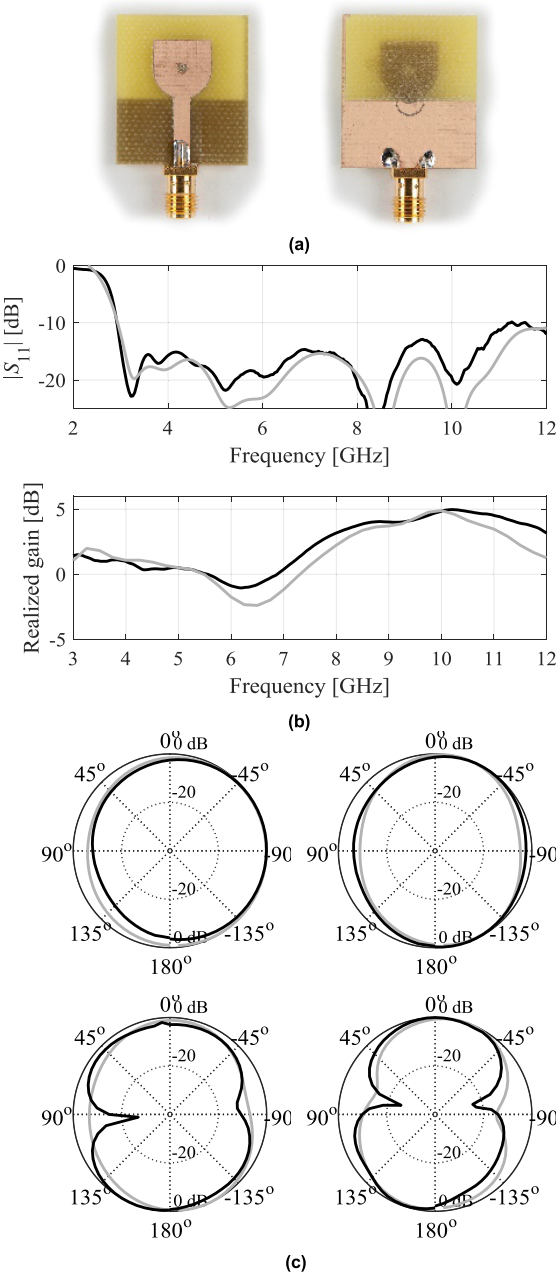


**FIGURE 5. Antenna of Fig. 3 optimized for $\varepsilon_r = 4.4$ and $h = 1.5$ mm, implemented on FR4 substrate: (a) antenna prototype, (b) reflection and realized gain, (c) H-plane patterns (4 GHz and 8 GHz), (d) E-plane patterns (4 GHz and 8 GHz); simulations (gray) and measurements (black).**

It can be observed that the initial design obtained from the first-level surrogate as $s_1(f_t)$ ($f_t$ being the target objective vector) is already excellent, so that surrogate optimization only brings relatively minor improvements. The design corresponding to $\varepsilon_r = 4.4$ and $h = 1.5$ mm (i.e., a popular FR4 substrate, widely used in antenna community) has been fabricated and measured for supplementary validation. Figure 5 shows the results with a good agreement between simulations and measurements.

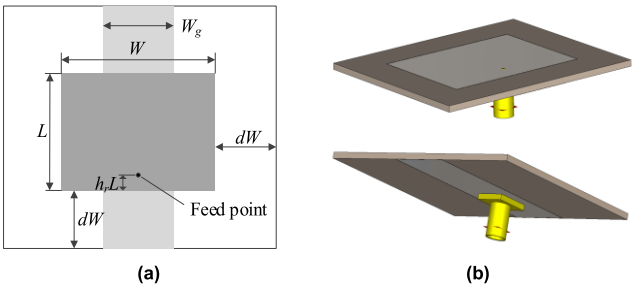


**FIGURE 6.** Broadband patch antenna [43]: (a) geometry (ground plane shown using light gray shade), (b) 3D views of the high-fidelity model with the SMA connector.

**TABLE 3.** Modeling results for patch antenna.

| Number of high-fidelity samples $N_f$ | Relative RMS error | | | | | | |
|---|---|---|---|---|---|---|---|
| | Conventional models | | Nested kriging model | Variable-fidelity nested co-kriging model [this work]* | | | |
| | kriging | RBF | | $N_f = 20$ $N_c = 400$ | $N_f = 50$ $N_c = 400$ | $N_f = 100$ $N_c = 400$ | $N_f = 50$ $N_c = 800$ |
| 50 | 43.4 % | 52.0 % | 10.1 % | | | | |
| 100 | 21.2 % | 25.4 % | 7.9 % | | | | |
| 200 | 16.0 % | 18.2 % | 7.2 % | 5.5 % [71#] | 4.3 % [101#] | 3.5 % [151#] | 4.1 % [152#] |
| 400 | 12.8 % | 14.7 % | 4.7 % | | | | |
| 800 | 9.8 % | 11.3 % | **3.3** % | | | | |

*$N_f$ and $N_c$ stand for the number of high- and low-fidelity samples, respectively.
#The number is brackets is the total equivalent number of $\boldsymbol{R}_f$ samples used to set up the surrogate (calculated as $N_f + N_c/m$ where $m$ is the time evaluation ratio between $\boldsymbol{R}_f$ and $\boldsymbol{R}_c$).

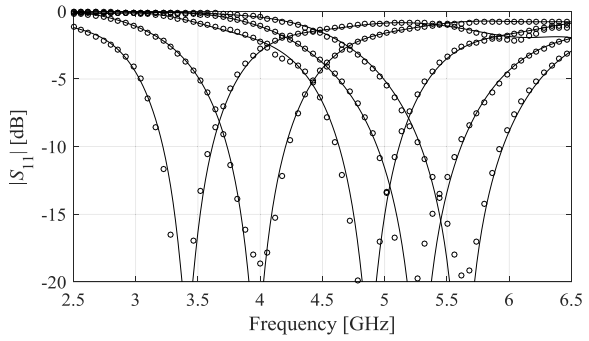


**FIGURE 7.** Reflection responses of the broadband patch antenna at the selected test designs: EM model (–), nested co-kriging surrogate with $N_f = 50$ and $N_c = 400$ (o).

### B. CASE II: BROADBAND PATCH ANTENNA

The second verification case is a broadband patch antenna with a narrow ground plane shown in Fig. 6 [43]. The design parameters are $\boldsymbol{x} = [WL\ dW\ W_g h_r]^T$. The EM models are implemented in CST Microwave Studio and evaluated using the transient solver: low-fidelity model $\boldsymbol{R}_c$ (∼75,000 mesh cells, simulation time 12 seconds), high-fidelity model $\boldsymbol{R}_f$ (∼400,000 cells, 94 seconds). The simulations were performed on Intel Xeon 2.1 GHz dual-core CPU, 128 GB RAM. The high-fidelity model contains the SMA connector, whereas the low-fidelity model is excited through a discrete port, which considerably reduces its simulation time while compromising the accuracy to a certain extent. The design optimality is understood as minimization of the antenna reflection within at least 10-percent fractional bandwidth symmetric w.r.t. the target center frequency $f_0$.

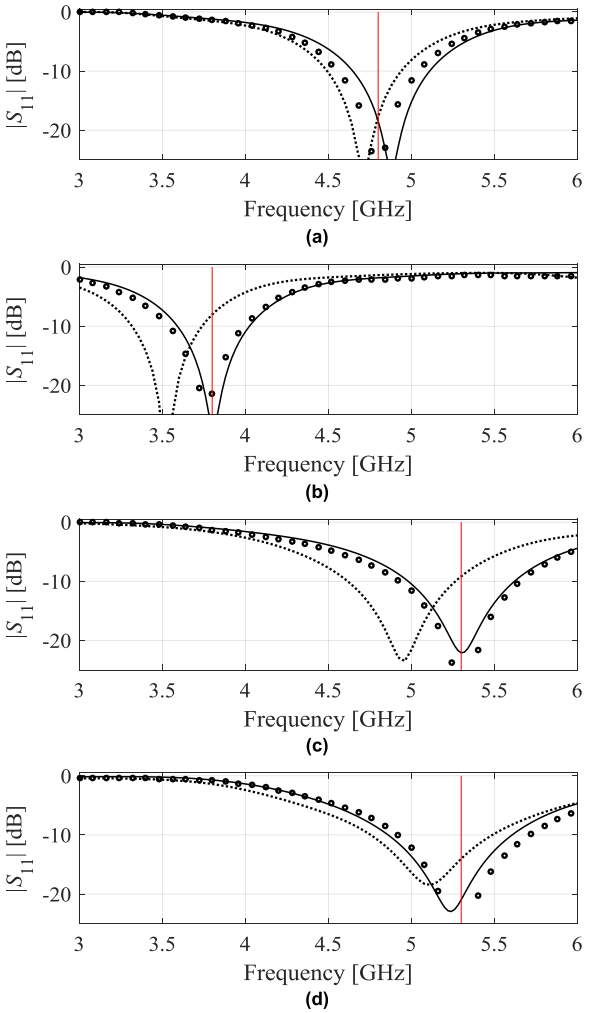


**FIGURE 8.** Reflection responses of the antenna of Fig. 6 optimized using the nested co-kriging surrogate set up with $N_f = 100$ and $N_c = 400$: initial design (· · ·), surrogate model response at the optimized design (o), EM simulated response (–): (a) $f_0 = 4.8$ GHz, $\varepsilon_r = 3.38$, $h = 0.51$ mm, (b) $f_0 = 3.8$ GHz, $\varepsilon_r = 2.5$, $h = 0.76$ mm, (c) $f_0 = 5.3$ GHz, $\varepsilon_r = 3.38$, $h = 0.81$ mm, (d) $f_0 = 5.3$ GHz, $\varepsilon_r = 4.4$, $h = 1.0$ mm. The red solid vertical line marks target operating frequency of the antenna.

The surrogate model is to be constructed valid for the following ranges of the center frequency and substrate parameters: 3.0 GHz $\leq f_0 \leq$ 6.0 GHz, permittivity 2.0 $\leq \varepsilon_r \leq$ 5.0 and height 0.5 mm $\leq h \leq$ 1.0 mm. The reference designs correspond to the following combinations of $\{f_0, \varepsilon_r, h\}$ = {3.0,2.0,0.5}, {3.0,2.0,1.0}, {3.0,5.0,0.5}, {3.0,5.0,1.0}, {4.5,3.5,0.75}, {4.5,3.5,0.5}, {4.5,3.5,1.0}, {4.5,2.0,0.75}, {4.5,5.0,0.75}, {6.0,2.0,0.5}, {6.0,2.0,1.0}, {6.0,5.0,0.5}, and {6.0,5.0,1.0}. The lower and upper bounds for design

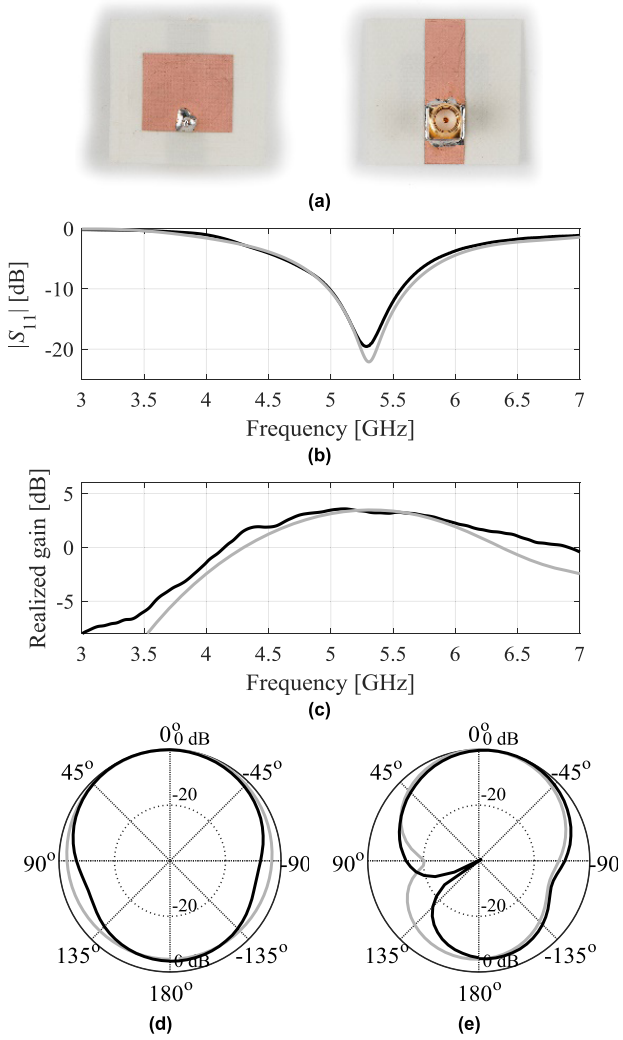


**FIGURE 9.** Antenna of Fig. 6 optimized for $f_0 = 5.3$ GHz, $\varepsilon_r = 3.38$ and $h = 0.81$ mm, implemented on RO4003 substrate: (a) antenna prototype, (b) reflection, (c) realized gain, (d) H-plane pattern at 5.3 GHz, (e) E-plane pattern at 5.3 GHz; simulations (gray) and measurements (black).

variables (i.e., the parameter space $X$) are $\boldsymbol{l} = [12.5\ 10.0\ 4.0\ 8.0\ 0.02]^T$, and $\boldsymbol{u} = [40.0\ 34.0\ 17.0\ 10.0\ 0.2]^T$.

Table 3 shows the numerical results obtained for the nested co-kriging surrogate as well as the benchmark methods (see also Fig. 7). Similarly as for the first example, the proposed model exhibits similar predictive power as the nested surrogate however, its setup cost is significantly lower. Table 4 and Fig. 8 show the results of application case studies, demonstrating suitability of the presented technique for design purposes. The design corresponding to $f_0 = 5.3$ GHz, $\varepsilon_r = 3.38$ and $h = 0.81$ mm has been fabricated on RO4003 laminate and measured for supplementary validation, see Fig. 9.

It should be noted, that the single- and variable-fidelity nested kriging surrogates are significantly better than the conventional ones both in terms of the model accuracy and the cost of the training data acquisition. This is because the latter are constructed within box-constrained domains defined by

**TABLE 4.** Broadband patch monopole: Optimization results.

| Operating conditions | | | Geometry parameter values [mm]* | | | | |
|---|---|---|---|---|---|---|---|
| $f_0$ [GHz] | $\varepsilon_r$ | $h$ [mm] | $W$ | $L$ | $dW$ | $W_g$ | $h_r$ |
| 4.8 | 3.38 | 0.51 | 19.8 | 16.6 | 6.87 | 7.97 | 0.04 |
| 3.8 | 2.5 | 0.76 | 26.7 | 23.7 | 9.73 | 8.07 | 0.15 |
| 5.3 | 3.38 | 0.81 | 17.4 | 15.0 | 6.41 | 7.95 | 0.09 |
| 5.3 | 4.4 | 1.0 | 15.0 | 13.1 | 5.48 | 7.97 | 0.09 |

* Variables with substripct *rel* are relative, i.e., unitless.

the lower and upper bounds on the parameters. Whereas, in most practical cases, the parameter sets corresponding to the high-quality designs with respect to the assumed performance specifications occupy a small subset of the original design space. Consequently, uniformly allocated samples in majority correspond to poor-quality designs. In the nested kriging technique, the modeling process is focused on the part of the design space containing useful designs. This dramatically limits the domain volume that needs to be sampled, hence, the training data set size can be significantly reduced, whereas the surrogate predictive power is high.

## IV. CONCLUSION

In the paper, a novel procedure for reliable surrogate modeling of antenna input characteristics has been proposed. Our approach combines domain confinement realized by the nested kriging method, and variable-fidelity EM simulations blended into the surrogate using co-kriging. Comprehensive benchmarking indicates superiority of the method over conventional models but also single-fidelity nested kriging in terms of the computational cost reduction while maintaining similar model accuracy. The achieved predictive power, making the models demonstrably suitable for design purposes, has been secured with the training data sets consisting of less than two hundred samples. It should be noted that the nested kriging approach requires certain initial effort related to acquisition of the reference designs. However, these designs (at least partly) may be available from the previous work with the same structure. Most importantly, this sort of cost may be unavoidable in the situations where conventional surrogates are simply insufficient to ensure required predictive power as this was actually the case for both verification cases considered in this work.

## ACKNOWLEDGMENT

The authors would like to thank Dassault Systemes, France, for making CST Microwave Studio available.

## REFERENCES

[1] N. Nguyen-Trong and C. Fumeaux, "Tuning range and efficiency optimization of a frequency-reconfigurable patch antenna," *IEEE Antennas Wireless Propag. Lett.*, vol. 17, no. 1, pp. 150–154, Jan. 2018.

[2] S. Manshari, S. Koziel, and L. Leifsson, "A wideband corrugated ridged horn antenna with enhanced gain and stable phase center for X- and ku-band applications," *IEEE Antennas Wireless Propag. Lett.*, vol. 18, no. 5, pp. 1031–1035, May 2019.

[3] S. Kim and S. Nam, "A compact and wideband linear array antenna with low mutual coupling," *IEEE Trans. Antennas Propag.*, vol. 67, no. 8, pp. 5695–5699, Aug. 2019.

[4] P. S. M. Yazeen, C. V. Vinisha, S. Vandana, M. Suprava, and R. U. Nair, "Electromagnetic performance analysis of graded dielectric inhomogeneous streamlined airborne radome," *IEEE Trans. Antennas Propag.*, vol. 65, no. 5, pp. 2718–2723, May 2017.

[5] U. Ullah and S. Koziel, "A broadband circularly polarized wide-slot antenna with a miniaturized footprint," *IEEE Antennas Wireless Propag. Lett.*, vol. 17, no. 12, pp. 2454–2458, Dec. 2018.

[6] M. A. Fakih, A. Diallo, P. Le Thuc, R. Staraj, O. Mourad, and E. A. Rachid, "Optimization of efficient dual band PIFA system for MIMO half-duplex 4G/LTE and full-duplex 5G communications," *IEEE Access*, vol. 7, pp. 128881–128895, 2019.

[7] S. K. Goudos, K. Siakavara, T. Samaras, E. E. Vafiadis, and J. N. Sahalos, "Self-adaptive differential evolution applied to real-valued antenna and microwave design problems," *IEEE Trans. Antennas Propag.*, vol. 59, no. 4, pp. 1286–1298, Apr. 2011.

[8] A. Lalbakhsh, M. U. Afzal, and K. P. Esselle, "Multiobjective particle swarm optimization to design a time-delay equalizer metasurface for an electromagnetic band-gap resonator antenna," *IEEE Antennas Wireless Propag. Lett.*, vol. 16, pp. 912–915, 2017.

[9] J. Zhang, C. Zhang, F. Feng, W. Zhang, J. Ma, and Q.-J. Zhang, "Polynomial chaos-based approach to yield-driven EM optimization," *IEEE Trans. Microw. Theory Techn.*, vol. 66, no. 7, pp. 3186–3199, Jul. 2018.

[10] A. Kouassi, N. Nguyen-Trong, T. Kaufmann, S. Lallechere, P. Bonnet, and C. Fumeaux, "Reliability-aware optimization of a wideband antenna," *IEEE Trans. Antennas Propag.*, vol. 64, no. 2, pp. 450–460, Feb. 2016.

[11] E. Hassan, D. Noreland, R. Augustine, E. Wadbro, and M. Berggren, "Topology optimization of planar antennas for wideband near-field coupling," *IEEE Trans. Antennas Propag.*, vol. 63, no. 9, pp. 4208–4213, Sep. 2015.

[12] J. Wang, X.-S. Yang, and B.-Z. Wang, "Efficient gradient-based optimisation of pixel antenna with large-scale connections," *IET Microw., Antennas Propag.*, vol. 12, no. 3, pp. 385–389, Feb. 2018.

[13] S. Koziel and A. Pietrenko-Dabrowska, "Variable-fidelity simulation models and sparse gradient updates for cost-efficient optimization of compact antenna input characteristics," *Sensors*, vol. 19, no. 8, p. 1806, 2019.

[14] S. Koziel and A. Pietrenko-Dabrowska, "Reduced-cost electromagnetic-driven optimisation of antenna structures by means of trust-region gradient-search with sparse jacobian updates," *IET Microw., Antennas Propag.*, vol. 13, no. 10, pp. 1646–1652, Aug. 2019.

[15] S. Koziel, "Fast simulation-driven antenna design using response-feature surrogates," *Int. J. RF Microw. Comput.-Aided Eng.*, vol. 25, no. 5, pp. 394–402, Jun. 2015.

[16] F. Feng, C. Zhang, W. Na, J. Zhang, W. Zhang, and Q.-J. Zhang, "Adaptive feature zero assisted surrogate-based EM optimization for microwave filter design," *IEEE Microw. Wireless Compon. Lett.*, vol. 29, no. 1, pp. 2–4, Jan. 2019.

[17] I. A. Baratta, C. B. de Andrade, R. R. de Assis, and E. J. Silva, "Infinitesimal dipole model using space mapping optimization for antenna placement," *IEEE Antennas Wireless Propag. Lett.*, vol. 17, no. 1, pp. 17–20, Jan. 2018.

[18] Y. Su, J. Li, Z. Fan, and R. Chen, "Shaping optimization of double reflector antenna based on manifold mapping," in *Proc. Int. Appl. Comp. Electromagn. Soc. Symp. (ACES)*, Suzhou, China, Aug. 2017, pp. 1–4.

[19] S. Koziel and S. D. Unnsteinsson, "Expedited design closure of antennas by means of Trust-Region-Based adaptive response scaling," *IEEE Antennas Wireless Propag. Lett.*, vol. 17, no. 6, pp. 1099–1103, Jun. 2018.

[20] J. A. Easum, J. Nagar, P. L. Werner, and D. H. Werner, "Efficient multiobjective antenna optimization with tolerance analysis through the use of surrogate models," *IEEE Trans. Antennas Propag.*, vol. 66, no. 12, pp. 6706–6715, Dec. 2018.

[21] A.-K.-S. O. Hassan, A. S. Etman, and E. A. Soliman, "Optimization of a novel nano antenna with two radiation modes using Kriging surrogate models," *IEEE Photon. J.*, vol. 10, no. 4, Aug. 2018, Art. no. 4800807.

[22] J. Dong, W. Qin, and M. Wang, "Fast multi-objective optimization of multi-parameter antenna structures based on improved BPNN surrogate model," *IEEE Access*, vol. 7, pp. 77692–77701, 2019.

[23] A. M. Alzahed, S. M. Mikki, and Y. M. M. Antar, "Nonlinear mutual coupling compensation operator design using a novel electromagnetic machine learning paradigm," *IEEE Antennas Wireless Propag. Lett.*, vol. 18, no. 5, pp. 861–865, May 2019.

[24] J. Tak, A. Kantemur, Y. Sharma, and H. Xin, "A 3-D-Printed W-Band slotted waveguide array antenna optimized using machine learning," *IEEE Antennas Wireless Propag. Lett.*, vol. 17, no. 11, pp. 2008–2012, Nov. 2018.

[25] S. Koziel and S. Ogurtsov, *Antenna Design by Simulation-Driven Optimization Surrogate-Based Approach*. New York, NY, USA: Springer, 2014.

[26] P. Barmuta, F. Ferranti, G. P. Gibiino, A. Lewandowski, and D. M. M.-P. Schreurs, "Compact behavioral models of nonlinear active devices using response surface methodology," *IEEE Trans. Microw. Theory Techn.*, vol. 63, no. 1, pp. 56–64, Jan. 2015.

[27] H. Liu, J.-R. Hervas, Y.-S. Ong, J. Cai, and Y. Wang, "An adaptive RBF-HDMR modeling approach under limited computational budget," *Struct. Multidisciplinary Optim.*, vol. 57, no. 3, pp. 1233–1250, Mar. 2018.

[28] J. A. Tropp and A. C. Gilbert, "Signal recovery from random measurements via orthogonal matching pursuit," *IEEE Trans. Inf. Theory*, vol. 53, no. 12, pp. 4655–4666, Dec. 2007.

[29] M. Kennedy, "Predicting the output from a complex computer code when fast approximations are available," *Biometrika*, vol. 87, no. 1, pp. 1–13, Mar. 2000.

[30] J. P. Jacobs and S. Koziel, "Two-stage framework for efficient Gaussian process modeling of antenna input characteristics," *IEEE Trans. Antennas Propag.*, vol. 62, no. 2, pp. 706–713, Feb. 2014.

[31] Y. Zhang, N. H. Kim, C. Park, and R. T. Haftka, "Multifidelity surrogate based on single linear regression," *AIAA J.*, vol. 56, no. 12, pp. 4944–4952, Dec. 2018.

[32] M. Giselle Fernández-Godino, C. Park, N. H. Kim, and R. T. Haftka, "Issues in deciding whether to use multifidelity surrogates," *AIAA J.*, vol. 57, no. 5, pp. 2039–2054, May 2019.

[33] X. Song, L. Lv, W. Sun, and J. Zhang, "A radial basis function-based multi-fidelity surrogate model: Exploring correlation between high-fidelity and low-fidelity models," *Structural Multidisciplinary Optim.*, vol. 60, no. 3, pp. 965–981, Sep. 2019.

[34] X. Ruan, P. Jiang, Q. Zhou, and Y. Yang, "An improved co-kriging multi-fidelity surrogate modeling method for non-nested sampling data," *Int. J. Mech. Eng. Robot. Res.*, vol. 8, no. 4, pp. 559–564, 2019.

[35] D. J. Perry, R. M. Kirby, A. Narayan, and R. T. Whitaker, "Allocation strategies for high fidelity models in the multifidelity regime," *SIAM/ASA J. Uncertainty Quantification*, vol. 7, no. 1, pp. 203–231, Jan. 2019.

[36] M. Shi, L. Lv, W. Sun, and X. Song, "A multi-fidelity surrogate model based on support vector regression," *Struct. Multidisc. Optim.*, to be published. [Online]. Available: https://link.springer.com/article/10.1007/s00158-020-02522-6, doi: 10.1007/s00158-020-02522-6.

[37] A. I. J. Forrester, A. Sóbester, and A. J. Keane, "Multi-fidelity optimization via surrogate modelling," *Proc. Roy. Soc. A, Math., Phys. Eng. Sci.*, vol. 463, no. 2088, pp. 3251–3269, Dec. 2007.

[38] L. Shu, P. Jiang, Q. Zhou, and T. Xie, "An online variable-fidelity optimization approach for multi-objective design optimization," *Struct. Multidisciplinary Optim.*, vol. 60, no. 3, pp. 1059–1077, Sep. 2019.

[39] S. Koziel, "Low-cost data-driven surrogate modeling of antenna structures by constrained sampling," *IEEE Antennas Wireless Propag. Lett.*, vol. 16, pp. 461–464, 2017.

[40] S. Koziel and A. T. Sigurdsson, "Triangulation-based constrained surrogate modeling of antennas," *IEEE Trans. Antennas Propag.*, vol. 66, no. 8, pp. 4170–4179, Aug. 2018.

[41] S. Koziel and A. Pietrenko-Dabrowska, "Performance-based nested surrogate modeling of antenna input characteristics," *IEEE Trans. Antennas Propag.*, vol. 67, no. 5, pp. 2904–2912, May 2019.

[42] M. G. N. Alsath and M. Kanagasabai, "Compact UWB monopole antenna for automotive communications," *IEEE Trans. Antennas Propag.*, vol. 63, no. 9, pp. 4204–4208, Dec. 2015.

[43] Y. Wang, Y. Lu, G. Lu, W. Cao, and A. A. Kishk, "Broadband patch antenna with narrow width ground plane," in *Proc. IEEE Int. Symp. Antennas Propag.*, Boston, MA, USA, Jul. 2018, pp. 8–13.

[44] S. N. Lophaven, H. B. Nielsen, and J. Søndergaard, "DACE: A MATLAB kriging toolbox," Tech. Univ. Denmark, Lyngby, Denmark, Tech. Rep. IMM-TR-2002-12, 2002.

**ANNA PIETRENKO-DABROWSKA** (Senior Member, IEEE) received the M.Sc. and Ph.D. degrees in electronic engineering from the Gdansk University of Technology, Poland, in 1998 and 2007, respectively. She is currently an Associate Professor with the Gdansk University of Technology. Her research interests include simulation-driven design, design optimization, control theory, modeling of microwave and antenna structures, and numerical analysis.

**SLAWOMIR KOZIEL** (Senior Member, IEEE) received the M.Sc. and Ph.D. degrees in electronic engineering from the Gdansk University of Technology, Poland, in 1995 and 2000, respectively, the M.Sc. degrees in theoretical physics and in mathematics, in 2000 and 2002, respectively, and the Ph.D. degree in mathematics from the University of Gdansk, Poland, in 2003. He is currently a Professor with the Department of Technology, Reykjavik University, Iceland. His research interests include CAD and modeling of microwave and antenna structures, simulation-driven design, surrogate-based optimization, space mapping, circuit theory, analog signal processing, evolutionary computation, and numerical analysis.